# $L_1$ to $N_5$ atomic level widths of thorium and uranium as inferred from measurements of $L$ and $M$ x-ray spectra

P.-A. Raboud, J.-Cl. Dousse, J. Hoszowska,* and I. Savoy
*Department of Physics, University of Fribourg, Ch. du Musée 3, CH-1700 Fribourg, Switzerland*
(Received 23 July 1999; published 13 December 1999)

High-resolution measurements of the photoinduced $L$ and $M$ x-ray spectra of metallic thorium and $M$ x-ray spectrum of metallic uranium were performed with transmission-type and reflection-type bent-crystal spectrometers. Linewidths of 31$L$ and 10$M$ x-ray emission lines of thorium and of 12$M$ x-ray emission lines of uranium were extracted. Using these results and those of Hoszowska *et al.* [Phys. Rev. A **50**, 123 (1994)] for the $L$ x rays of uranium, by means of a least-squares method we have determined the level widths of the subshells $L_1$ to $N_5$ of thorium and uranium.

PACS number(s): 32.70.Jz, 32.30.Rj, 32.80.Fb

## I. INTRODUCTION

Atomic level widths and related x-ray linewidths are of interest and value in several respects. For high-resolution x-ray spectroscopy, a precise knowledge of x-ray linewidths is very helpful because it permits one to improve data analysis by diminishing the number of free-fitting parameters and anchoring the natural linewidths of the observed transitions to known values. This results in improved accuracy in x-ray emission techniques such as high-resolution x-ray fluorescence and particle-induced x-ray emission [1–3]. Furthermore, in a variety of experiments in which weak structures have to be extracted from the tails of close-lying and much stronger diagram transitions, the line shapes of the latter must be known accurately to obtain reliable results. Radiative Auger transitions [4–8] are examples of such weak structures sitting on the low-energy tails of intense diagram lines. Satellite x rays that originate from the radiative decay of multiple-vacancy states are often poorly separated from their parent diagram line. In this case, also, the energy and yield of the satellite line can be fitted in a reliable way only if the width of the Lorentzian representing the natural line shape of the neighboring main line is known precisely [9]. As shown in Ref. [10], even in low-resolution Si(Li) spectra, the lifetime broadening inherent to atomic transitions makes a significant contribution to the low- and high-energy tails of the peaks. A high-precision fit of such spectra again needs a good knowledge of the natural broadening. Accurate and reliable experimental data concerning atomic level widths are also important because they provide a sensitive test of theoretical models. In particular, they are of interest to probe the goodness of theoretical predictions concerning total vacancy lifetimes, radiative and radiationless transition probabilities, or fluorescence yields. In some calculations they are also used to adjust the parameters of the theoretical model.

Precise results for the linewidths of $L$ and $M$ x rays are scarce, and discrepancies exist between the few existing experimental data and the theoretical predictions. Experimentally reliable results can only be obtained with instruments whose resolution is comparable to the natural linewidths of the transitions to be measured. In x-ray spectrometry this restricts the choice of instruments to crystal spectrometers. The lack of accurate experimental data concerning $L$ x rays of heavy elements is probably due to the fact that the photon energy region between 10 and 20 keV is rather unfavorable for crystal diffractometry measurements. Transmission-type crystal spectrometers are operated mostly above 20 keV, while reflection-type ones are generally used below 10 keV. Crystal spectrometers are characterized by high resolution and high precision. Their luminosity, however, remains small as compared to semiconductor detectors. For $M$ x rays high-resolution crystal spectroscopy is therefore handicapped by the poor intensity of the $M$ x-ray emission lines. Even for heavy elements, the fluorescence yields for the $M$ shell is indeed about 100 times smaller than for the $K$ shell.

In this paper we report on the natural widths of the $L_1$ to $N_5$ atomic levels in metallic thorium and metallic uranium. The level widths were obtained from the natural linewidths of a number of $L$ and $M$ x-ray lines measured by means of high-resolution crystal spectroscopy. From the transition widths determined in the present experiment and the $L$ x-ray linewidths obtained for uranium in a similar previous work [11], two self-consistent sets of simultaneous equations with the level widths as unknowns could be built for thorium and uranium. Assuming that core levels are only weakly influenced by nonlifetime broadening effects, the natural widths of the levels $L_1$ to $N_5$ were then determined by solving the sets of linear equations by means of a least-squares method. Results given in the present paper are not, however, solely limited to the widths of atomic levels. Linewidths and energies of numerous $L$ x-ray lines of thorium and $M$ x-ray lines of thorium and uranium are also presented. To our knowledge, the natural linewidths of most transitions were determined experimentally for the first time. The results obtained in the present work are compared to other experimental data, where available, and theoretical predictions based principally on the independent-particle model.

## II. EXPERIMENT

The measurements of the x-ray spectra were performed at the University of Fribourg by means of high-resolution x-ray

*Present address: European Synchrotron Radiation Facility (ESRF), 156 rue des Martyrs, F-38043 Grenoble, France.

 

spectroscopy. The $L$ x-ray emission spectrum of thorium was observed with a Dumond transmission-type crystal spectrometer. As this instrument cannot be used for photon energies below about 10 keV, the $M$ x-ray emission lines of thorium and uranium were measured with a von Hamos reflection-type crystal spectrometer. For both elements, the fluorescence x-ray spectra were produced by irradiating the targets with the bremsstrahlung of an x-ray tube.

### A. $L$ x-ray emission spectrum of thorium

The main characteristics of the Dumond curved crystal spectrometer of Fribourg were already presented in several previous papers (see, e.g., Refs. [11,5,6,12]). Thus, in the following, only the features specific to the experimental setup used for the measurement of the $L$ x-ray emission spectrum of thorium will be discussed.

The spectrometer was operated in a so-called modified DuMond slit geometry. In this geometry the target is viewed by the bent crystal through a narrow slit located on the focal circle. The 0.1-mm-wide vertical rectangular slit was made of two 5-mm-thick juxtaposed Pb plates. A 25-mm-high by 4-mm-wide by 0.5-mm-thick self-supported metallic target of thorium was used. The target $L$ x-ray emission was induced by means of an Au x-ray tube operated at 80 kV and 35 mA. The distance between the tube anode and the target center was 4.5 cm, and the axis of the conical beam emitted by the x-ray tube was perpendicular to the target-crystal direction. In order to avoid a contamination of the thorium spectrum due to a coherent scattering by the target of a number of characteristic Au $L$ x-ray lines from the tube anode, a 250-mg/cm$^2$-thick aluminum absorber was placed between the tube and the target for the measurements of the $L_3$-$M_1$, $L_3$-$M_4$, and $L_3$-$M_5$ transitions of thorium.

For the diffraction of the x rays the (110) reflecting planes of a $10\times10$-cm$^2$ quartz-crystal plate, 0.5 mm thick, were used. The quartz lamina was bent to a radius $R=311.1$ cm by means of a bending device similar to the one described in Ref. [13]. The effective reflecting area of the crystal was 12 cm$^2$. The Bragg angles, i.e., the angles between the incident x-ray radiation and the reflecting planes of the crystal were measured by means of an optical laser interferometer with a precision of $3-5\times10^{-3}$ arcsec [14].

The instrumental response of the spectrometer which depends mainly on the slit width and precision of the crystal curvature was determined by measuring the $K\alpha_1$ transition of Au whose energy and natural linewidth were taken from Ref. [15]. From this calibration measurement the instrumental angular broadening was found to be well reproduced by a Gaussian profile of 15.2 arcsec full width at half maximum (FWHM). Over the energy range covered by the $L$ x-ray lines of thorium, the corresponding energy resolution of the spectrometer varied thus between 3.5 eV for the $L_3$-$M_1$ transition (11.118 keV) and 12.1 eV for the $L_1$-$P_{2,3}$ transition (20.450 keV).

In the DuMond slit geometry, the best angular resolution is obtained when the slit-to-crystal distance is adjusted for each x-ray line. However, when the x-ray spectrum extends over a large angular range and comprises many weak lines, this optimization is not so convenient. It is more practical to measure a selected group of lines with an average value of focusing distance. As a consequence, only a slightly worse instrumental resolution results. In fact the smooth variation of the instrumental broadening as a function of the focusing distance was determined with the Au $K\alpha_1$ transition, and then used to compute the actual instrumental width corresponding to each particular thorium $L$ x-ray line.

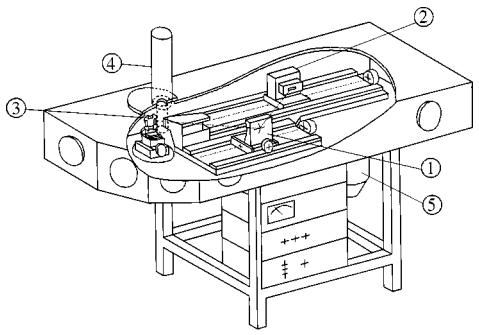


FIG. 1. Schematic view of the von Hamos spectrometer: (1) crystal, (2) CCD detector, (3) target barrel, (4) x-ray tube, and (5) vacuum pump.

For the energy calibration of the spectrum, the lattice spacing constant of the (110) reflecting planes and the angular position of the zero Bragg angle are needed. The lattice spacing constant was deduced from the above-mentioned $K\alpha_1$ line of Au measurement, giving a value of 2.456624(7) Å. The zero Bragg angle may change when varying the focusing distance. For that reason, it was determined for each group of lines observed at the same focusing distance, by measuring the most intense line of the group at positive and negative Bragg angles.

For the detection of the x rays, a 5-in.-diam by 0.25-in. NaI(Tl) by 2-in. CsI(Tl) Phoswich (The Harshaw Chemical Co., Crystal and Electronic Products Dept., OH 94139) scintillation detector was employed. This type of detector strongly reduces the Compton noise arising from high-energy photons [11]. A further reduction of the background was achieved by enclosing the Phoswich detector in heavy Pb-Cu-Al shielding, and by sorting on line the events of interest as a function of their energy. In order to reduce the absorption of x rays in air, evacuated tubes were mounted between the target and the crystal and between the crystal and the 66-cm-long Soller-slit collimator. The latter and the target chamber were also pumped down to about 1 mbar.

### B. $M$ x-ray emission spectra of thorium and uranium

As the observation of photons below 10 keV requires a reflecting-type x-ray spectrometer, the measurements of the $M$ x-ray emission spectra of thorium and uranium were performed with a von Hamos curved crystal facility [16]. The principal elements of this instrument are an x-ray source defined by a rectangular slit, a cylindrically bent crystal, and a position-sensitive detector (see Fig. 1). In the von Hamos geometry the crystal is bent around an axis which is parallel to the direction of dispersion, and provides focusing in the nondispersive direction. For a fixed position of the compo-

nents, the impact coordinate on the detector of a reflected x-ray corresponds geometrically to a particular Bragg angle, and hence to a particular photon energy. Such a geometry, at one position of the spectrometer components, permits data collection over an energy bandwidth which is limited by the detector length. In order to study a greater energy interval, the central Bragg angle is adjusted by translation of the crystal and correspondingly of the detector along their axes. The slit-to-crystal and crystal-to-detector distances are varied but kept equal. The target, crystal, and detector are all contained in a $180\times62\times24.5$-cm$^3$ stainless steel vacuum chamber, which can be pumped down to about $10^{-7}$ mbar by a turbomolecular pump.

The Bragg angle domain covered by the von Hamos spectrometer extends from 24.4° to 61.1°, so that two different crystals were needed for the coverage of the ~6-keV-wide energy domain corresponding to the $M$ x rays of thorium and uranium. A $(1\bar{1}0)$ quartz crystal ($2d=8.5096$ Å) was employed for the observation of the transitions below 3.5 keV, and a (200) LiF crystal ($2d=4.0280$ Å) for transitions at higher energies. Both crystals, 10 cm high by 5 cm wide by 0.5 mm thick, were glued to Al blocks machined to a precise concave cylindrical surface with a nominal bending radius of 25.4 cm.

The vertical rectangular slit consisted of two juxtaposed Ta pieces 0.3 mm thick and 10 mm high. The slit width was 50 $\mu$m for all measurements. A 25-mm-high by 4-mm-wide metallic target of natural uranium, 48 mg/cm$^2$ thick, and a 24-mm-high by 10-mm-wide metallic target of thorium, 575 mg/cm$^2$ thick, were used. The target $M$ x-ray emission was induced by means of a Cr anode x-ray tube operated at 60 kV and 40 mA.

The x rays were recorded with a CCD (charged-coupled device) position-sensitive detector 27.65 mm long and 6.9 mm high, having a depletion depth of 50 $\mu$m and consisting of 1024 columns and 256 rows with a pixel size of $27\times27$ $\mu$m$^2$. The diffracted x rays hitting the CCD build a two-dimensional pattern on the detector plane. The horizontal axis of the detector corresponds to the energy axis of the x-ray spectrum, while the vertical extension of the detector serves mainly to collect more intensity. The CCD detector was thermoelectrically cooled down to $-60\,^\circ$ C. It was operated by a ST-138 controller (Princeton Instrument, Inc.) equipped with a DMA/TAXI high-speed serial interface which can sustain data transfer to a personal computer at 1 Mbyte/sec.

For data acquisition and analysis of images, a dedicated software package written specifically to operate the ST-138 controller was used. The time of a single acquisition was chosen depending on the count rate, so that multiple hits on one pixel were minimized. Thanks to the good energy resolution of the CCD detector, higher-order reflections and background events could be rejected by setting appropriate energy windows. The data were taken in a repetitive accumulation mode. Each image corresponding to a separate acquisition was filtered. Then the different images were summed and the resulting two-dimensional spectrum was projected on the axis of dispersion to give the one-dimensional position spectrum.

The energy calibration of the spectrometer and the determination of the instrumental response were performed by measuring the $K\alpha_1$ x-ray lines of Ar, Ca, Sc, Ti, and V. The natural linewidths and energies of the $K$ transitions were taken from Refs. [17,18], respectively. It was found that for both crystals the instrumental response could be well reproduced by a Gaussian profile whose width (FWHM) varied as a function of the x-ray energy between 1.0 and 1.3 eV.

## III. DATA ANALYSIS

The $L$ and $M$ x-ray spectra were analyzed by means of the least-squares-fitting computer code MINUIT [19]. As the convolution of the Gaussian instrumental broadening with the Lorentzian representing the natural line shape of an x-ray transition results in a so-called Voigt function, such Voigt profiles were employed to fit the observed spectral lines. The natural widths of the x-ray lines of interest were extracted by keeping fixed in the fit the known Gaussian experimental broadening. The energies and intensities of the transitions as well as the linear background were used as additional free fitting parameters.

The $M$ and $N$ satellite structures observed on the high-energy tails of the $L_3$, respectively $M_3$ to $M_5$ diagram transitions could also be fitted satisfactorily with Voigt functions. However, because these satellite structures consist in general of numerous overlapping components many of them had to be fitted with several Voigt profiles. Average energy shifts of $L$ x rays due to $M$ spectator vacancies are reported in Ref. [20]. We have used these theoretical predictions in the analysis to identify the satellites accompanying the observed $L_3$ x rays lines. A clear example of $M$ satellite structure can be seen on the high-energy side of the $L_3$-$N_5$ transition represented in Fig. 2(a).

In certain spectra a strong overlap of distinct diagram lines made the analysis more difficult and the results of the latter less reliable. Such problems were encountered, for instance, in the fit of the $L$ x-ray spectrum of thorium with the close-lying $L_3$-$N_{4,5}$ and $L_1$-$M_2$ transitions [see Fig. 2(a)] and $L_2$-$M_4$ and $L_3$-$O_{4,5}$ transitions [see Fig. 3(a)]. The energy differences between the two lines are in both cases smaller than the natural widths of the overlapping transitions. The difficulty was solved in the following way. First, the problematic energy regions were remeasured by operating the x-ray tube at 20.4 [see Fig. 2(b)] and 19.6 [see Fig. 3(b)] kV, respectively, i.e., at voltage values just below the $L_1$ and $L_2$ edges of thorium. These spectra could then be analyzed properly since they were no longer affected by the overlap problem. Finally, the 80-kV spectra could also be fitted successfully by keeping the energies and linewidths of the $L_3$ transitions at the values obtained from the analysis of the 20.4- and 19.6-kV spectra fixed in the fitting procedure.

## IV. RESULTS AND DISCUSSION

### A. $L$ x-ray lines of thorium

The values of the natural linewidths and energies of the 31$L$ x-ray transitions of thorium observed in the present study are listed in Tables I and II, respectively. Our results

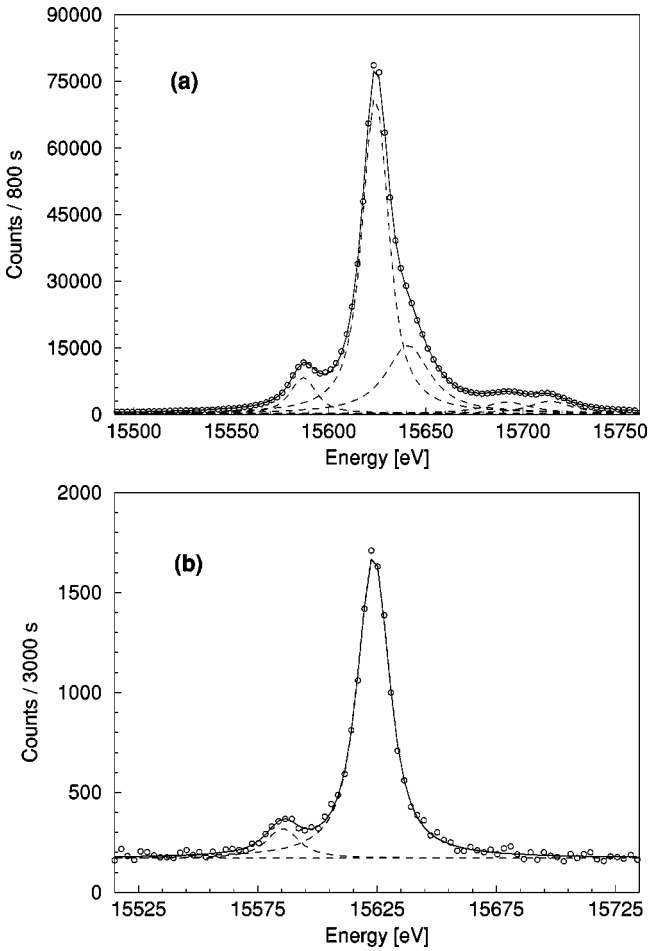


FIG. 2. The $L_3$-$N_4$ (15587 eV), $L_3$-$N_5$ (15624 eV), and $L_1$-$M_2$ (15640 eV) transitions of thorium with the accompanying $M$ satellite structure components shifted by 68 and 90 eV with respect to the $L_3$-$N_5$ line. The $L$ emission was induced with the x-ray tube operated at (a) 80 and (b) 20.4 kV.

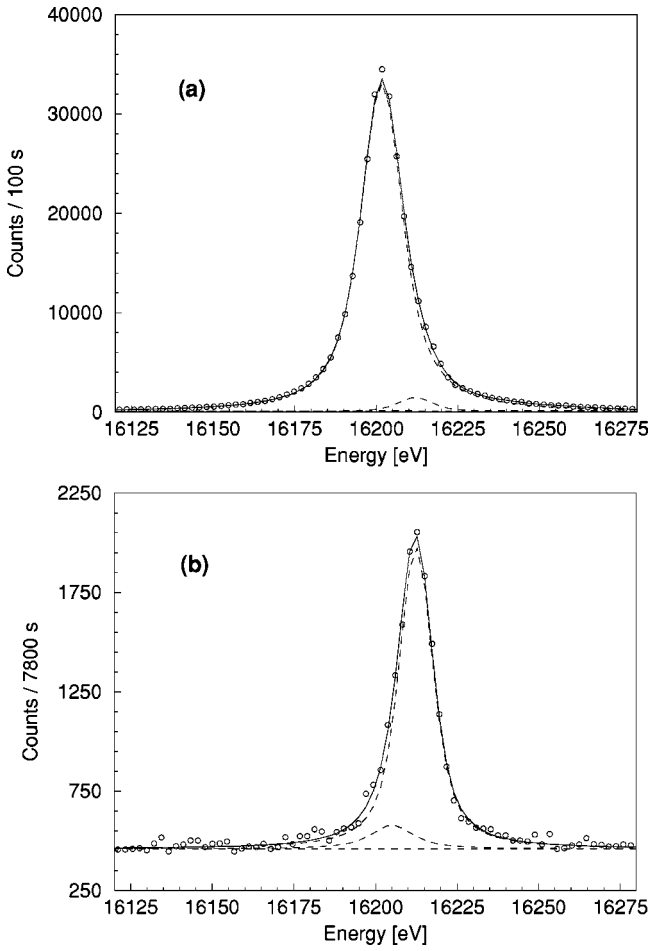


FIG. 3. The $L_2$-$M_4$ (16202 eV) and $L_3$-$O_{4,5}$ (16205 and 16212 eV) transitions of thorium. The $L$ emission was induced with the x-ray tube operated at (a) 80 and (b) 19.6 kV.

are compared to other available experimental data and theoretical predictions. The theoretical x-ray linewidths were determined from the sum of the widths of the two levels involved in the transitions, using results of McGuire's calculations [21–23] for $L$, $M$, and $N$ atomic level widths. It has to be noted that the errors quoted in Tables I and II are only statistical errors obtained from the error matrix of the least-squares-fit program, and that they do not include the smaller but nonvanishing systematic errors inherent to the experimental method and instruments employed in our investigations.

From Table I one can notice first that existing experimental information about the natural linewidths of the $L$ x-ray transitions in thorium is rare and concerns only the most intense lines. The values quoted in the third column were taken from the tabulation of Salem and Lee [17]. They are based on relatively old measurements performed in 1961 by Merill and DuMond [24] with a double-crystal spectrometer. Errors concerning these measurements were not reported, but they were estimated by Salem and Lee to be 10% or more. The average of the absolute values of the differences between our results and those of Merill and DuMond is only 0.7 eV or 5%, thus indicating that already in these pioneering works of crystal spectroscopy remarkable results were obtained. A similar good agreement is observed between our results and the experimental values published more recently by Amorim *et al.* [25]. In this case the mean value of the relative differences is about 4%. In contrast to that, a comparison with the values listed in the last column on the right seems to indicate that theory is in disagreement with our results. However, if we consider that the theoretical x-ray linewidths were determined by adding the natural widths of the two levels participating in the transition, and that the width of each of these two levels was computed from the sum of the calculated radiative, Auger, and Coster-Kronig widths, the observed differences are more understandable. In fact, theory overestimates significantly only the widths of those transitions in which an $s$ level (i.e., an $X_1$ subshell) is involved. This observation indicates that the Coster-Kronig yields calculated by McGuire are probably too large.

Examining now the values of the experimental linewidths obtained in the present study, one can see that the expected general trend $\Gamma_{L_1Y_k} > \Gamma_{L_2Y_k} \geqslant \Gamma_{L_3Y_k}$ attributed to the decrease in Coster-Kronig-Auger decay rates with increasing angular momentum is in general well verified. An important question on which we will focus in the following is to know whether

TABLE I. Natural linewidths in (eV) of photoinduced $L$ x-ray emission lines of thorium. Our experimental results are compared to existing experimental data (Expt.) and theoretical predictions (Calc.).

| Line | This experiment | Ref. [17] Expt. | Ref. [25] Expt. | Ref. [21–23] Calc. |
|---|---|---|---|---|
| $L_1$-$M_2$ | 27.6±0.7 | 26.4 | | 35.9 |
| $L_1$-$M_3$ | 23.6±0.3 | 22.9 | 21.5 | 33.3 |
| $L_1$-$M_4$ | 17.6±0.5 | | | 23.6 |
| $L_1$-$M_5$ | 17.0±0.3 | | | 23.3 |
| $L_1$-$N_2$ | 23.3±0.1 | | | 28.7 |
| $L_1$-$N_3$ | 22.6±0.1 | | | 27.9 |
| $L_1$-$N_4$ | 16.1±2.5 | | | 25.7 |
| $L_1$-$N_5$ | 16.8±1.6 | | | 25.7 |
| $L_1$-$O_2$ | 22.2±1.2 | | | |
| $L_1$-$O_3^I$ | 22.8±1.2 | | | |
| $L_1$-$O_3^{II}$ | 18.9±0.6 | | | |
| $L_1$-$O_{4,5}$ | 13.8±2.3 | | | |
| $L_1$-$P_{2,3}$ | 19.9±0.6 | | | |
| $L_2$-$M_1$ | 23.1±0.2 | | | 34.0 |
| $L_2$-$M_4$ | 11.6±0.1 | 12.4 | 11.2 | 14.5 |
| $L_2$-$M_5$ | 11.7±2.4 | | | 14.2 |
| $L_2$-$N_1$ | 19.2±0.4 | | | 22.5 |
| $L_2$-$N_4$ | 13.3±0.1 | 15.0 | 14.4 | 16.6 |
| $L_2$-$N_6$ | 8.6±0.6 | | | 11.5 |
| $L_2$-$O_1^I$ | 29.9±0.2 | | | |
| $L_2$-$O_1^{II}$ | 29.4±0.5 | | | |
| $L_2$-$O_4$ | 8.5±0.1 | | | |
| $L_3$-$M_1$ | 23.5±0.5 | | 24.3 | 29.7 |
| $L_3$-$M_4$ | 11.8±0.1 | 11.9 | 11.8 | 10.2 |
| $L_3$-$M_5$ | 12.0±0.1 | 11.8 | 11.8 | 9.9 |
| $L_3$-$N_1$ | 19.3±0.1 | | | 18.2 |
| $L_3$-$N_4$ | 12.1±0.2 | | | 12.2 |
| $L_3$-$N_5$ | 12.5±0.1 | 12.8 | 12.7 | 12.2 |
| $L_3$-$N_6$ | 7.6±1.2 | | | 7.1 |
| $L_3$-$N_7$ | 7.6±0.7 | | | |
| $L_3$-$O_1^I$ | 26.0±2.2 | | | |
| $L_3$-$O_1^{II}$ | 23.5±2.4 | | | |
| $L_3$-$O_4$ | 12.3±4.0 | | | |
| $L_3$-$O_5$ | 8.3±0.3 | | | |

nonlifetime broadening effects influence the natural linewidths of the presently investigated thorium lines and, if yes, to what extent our results are affected by such effects. A review of the possible broadening contributions can be found in Ref. [26]. In our experiment the main contributions are associated with the occurrence of multivacancy states in the decaying atoms, and with exchange interactions between core holes and unpaired valence electrons.

The energy of so-called x-ray satellite lines emitted by atoms which have more than one inner-shell vacancy in their initial and final states is generally slightly higher than that of the parent diagram x rays, which are associated with initial and final states of single-hole configurations. The energy difference between a satellite and its parent diagram line is found to decrease with the principal quantum number of the spectator vacancy, i.e., the vacancy not involved in the transition. As a consequence, the radiative decay of $LM$ states gives rise to resolved satellites, whereas that of $LN$ states results only in a broadening of the parent diagram line. Extensive calculations concerning the energies of $L$ x-ray satellites of thorium with one spectator vacancy in the $M$ or $N$ shell (hereafter called $M$ or $N$ satellites) can be found in Ref. [27]. The energy shifts of $O$ and $P$ satellites are much smaller and their influence on the $L$ x-ray linewidths can thus be neglected. In other words, our experimental linewidths of $L$ transitions may be affected in a sizable way only by satellites related to spectator vacancies located in the $N$ shell.

In photoinduced $L$ x-ray spectra, satellite lines may be induced by $LLX$ Coster-Kronig transitions and shakeoff processes, while direct multiple ionization can be considered as negligibly small. For thorium, $L_1L_2N_{4-7}$, $L_1L_3N_{1-7}$, and $L_2L_3N_{1-7}$ Coster-Kronig transitions are allowed, from which $L_2N_k$ and $L_3N_k$ doubly ionized states result. Taking into account the probabilities for $L_jL_3N_k$ Coster-Kronig transitions

TABLE II. Energies in (eV) of photoinduced $L$ x-ray emission lines of thorium. Our experimental results are compared to the data from two experiments (Expt.) and one theory (Calc.).

| Line | This experiment | Ref. [18] Expt. | Ref. [32] Expt. | Ref. [33] Calc. |
|---|---|---|---|---|
| $L_1$-$M_2$ | 15639.64±0.35 | 15642.9 | 15639.5 | 15641.0 |
| $L_1$-$M_3$ | 16423.96±0.07 | 16425.8 | 16424.0 | 16426.0 |
| $L_1$-$M_4$ | 16980.37±0.21 | 16981.0 | 16979.4 | 16981.0 |
| $L_1$-$M_5$ | 17139.00±0.12 | 17139.0 | 17138.0 | 17140.0 |
| $L_1$-$N_2$ | 19303.11±0.05 | 19305.0 | 19301.8 | 19304.0 |
| $L_1$-$N_3$ | 19503.57±0.06 | 19507.0 | 19502.5 | 19504.0 |
| $L_1$-$N_4$ | 19756.88±0.83 | 19755.0 | 19755.7 | 19758.0 |
| $L_1$-$N_5$ | 19794.04±0.50 | 19794.0 | 19793.7 | 19795.0 |
| $L_1$-$O_2$ | 20236.52±0.18 | 20242.0 | 20245.0 | 20243.0 |
| $L_1$-$O_3^I$ | 20272.10±0.66 | | | |
| $L_1$-$O_3^{II}$ | 20290.66±0.27 | 20292.0 | 20288.2 | 20290.0 |
| $L_1$-$O_{4,5}$ | 20381.03±0.97 | 20383.0 | | |
| $L_1$-$P_{2,3}$ | 20450.39±0.28 | 20424.0 | 20426.0 | |
| $L_2$-$M_1$ | 14510.42±0.08 | 14509.0 | 14509.8 | 14511.0 |
| $L_2$-$M_4$ | 16201.66±0.03 | 16202.2 | 16201.4 | 16202.0 |
| $L_2$-$M_5$ | 16358.20±1.00 | 16359.0 | 16360.0 | 16361.0 |
| $L_2$-$N_1$ | 18364.47±0.11 | 18370.0 | 18362.3 | 18363.0 |
| $L_2$-$N_4$ | 18978.38±0.02 | 18982.5 | 18977.7 | 18979.0 |
| $L_2$-$N_6$ | 19348.12±0.15 | 19353.0 | 19347.9 | 19349.0 |
| $L_2$-$O_1^I$ | 19395.21±0.52 | | | |
| $L_2$-$O_1^{II}$ | 19408.89±0.51 | 19403.0 | 19402.0 | 19403.0 |
| $L_2$-$O_4$ | 19597.16±0.02 | 19599.0 | 19597.6 | 19598.0 |
| $L_3$-$M_1$ | 11118.13±0.18 | 11118.6 | 11117.6 | 11118.0 |
| $L_3$-$M_4$ | 12809.58±0.03 | 12809.6 | 12809.2 | 12810.0 |
| $L_3$-$M_5$ | 12968.02±0.02 | 12968.7 | 12967.8 | 12968.0 |
| $L_3$-$N_1$ | 14973.52±0.05 | 14975.0 | 14970.1 | 14970.0 |
| $L_3$-$N_4$ | 15587.01±0.07 | 15587.5 | 15585.5 | 15586.0 |
| $L_3$-$N_5$ | 15624.06±0.03 | 15623.7 | 15623.5 | 15623.0 |
| $L_3$-$N_6$ | 15955.95±0.58 | 15964.0 | 15955.7 | 15956.0 |
| $L_3$-$N_7$ | 15965.98±0.58 | 15964.0 | 15964.9 | 15965.0 |
| $L_3$-$O_1^I$ | 16006.52±0.63 | 16010.5 | 16009.8 | 16010.0 |
| $L_3$-$O_1^{II}$ | 16024.27±0.63 | | | |
| $L_3$-$O_4$ | 16205.12 [a] | | 16205.4 | 16205.0 |
| $L_3$-$O_5$ | 16212.40±0.14 | | 16211.7 | 16213.0 |

[a]Value kept fixed in the fit according to the energy difference determined from the $M_3$-$O_{4,5}$ transition.

quoted in Ref. [28] and the weighted energy shifts of the $N_k$ satellite components from Ref. [27], we found, for instance, that the average energy shift $E(L_3N^0\text{-}M_1N^0) - E(L_3N^1\text{-}M_1N^1)$ of the $N$ satellite of the $L_l$ transition is 3.2 eV. Similarly we found for the average energy shift of the $L_l$ $M$ satellite produced, via $L_1L_3M_{4,5}$ Coster-Kronig transitions, a value of 39.5 eV which is in quite satisfactory agreement with the value of 36.0±2.0 eV extracted from our measurements. From the fitted relative intensity of the $M$ satellite (19%) and the ratio $\Sigma_{j=1}^{2}\Sigma_{k=1}^{7}P_{CK}(L_jL_3N_k):\Sigma_{l=4}^{5}P_{CK}(L_1L_3M_l)$ of the Coster-Kronig (CK) probabilities $P_{\mathrm{CK}}$ taken from Ref. [28], a relative intensity of about 7.5% with respect to the diagram line is expected for the $N$ satellite. Assuming furthermore that the width of the $N$ satellite is similar to that of the $M$ satellite, for which a value of 44±5 eV was obtained from the data analysis, the natural linewidth and energy of the pure $L_l$ diagram transition can be determined by subtracting from the measured profile the $N$ satellite line. The new value obtained for the linewidth is 23.2 eV, i.e., only 0.3 eV smaller than the result given in Table I. The change in the energy is −0.04 eV, which is also negligible with respect to the quoted uncertainty of 0.18 eV. It can thus be concluded that the experimental linewidths of the $L_3$ and, *a fortiori*, those of the $L_2$ x rays determined in the present study are only weakly increased by the unresolved $N$ satellites originating from Coster-Kronig transitions, the $L_1$ x rays not being influenced at all by this nonlifetime broadening effect.

In photoionization double-vacancy states may also arise from shake processes. As a consequence of the abrupt change of the atomic potential following the removal of a core electron by photon impact, other bound electrons can

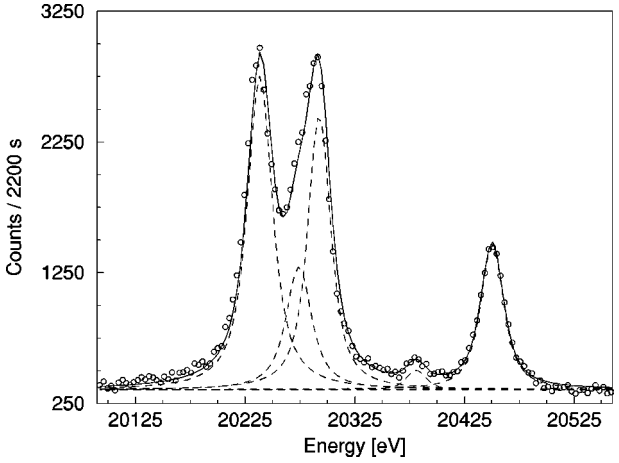


FIG. 4. The $L_1$-$O_2$ transition of thorium at 20236 eV, the two splitting components of $L_1$-$O_3$ at 20272 and 20291 eV, respectively, and the $L_1$-$O_{4,5}$ and $L_1$-$P_{2,3}$ emission lines.

indeed be ejected into the continuum (shakeoff) or promoted to higher unoccupied bound states (shakeup). The shakeup to shakeoff probability ratio decreases rapidly with increasing atomic number *Z*, so that for heavy elements like thorium only the shakeoff process must be considered. Predictions for shakeoff probabilities in different subshells when a single hole is created in the *L* shell were reported for iridium, gold, and uranium in Ref. [29]. The calculations were performed within the frame of the sudden approximation method [30,31]. From an interpolation of the results quoted in Ref. [29], probabilities for shakeoff processes in the *M* and *N* shells of thorium were found to be 0.13% and 1.84%, respectively. The very small shakeoff probability predicted for the *M* shell is well confirmed by our data which do not reveal any *M* satellite structure for the transitions to the $L_1$ level nor to the $L_2$ one [see, e.g., Fig. 3(a)]. The *N*-shell shake probability is more than ten times larger, but its contribution to the *N* satellite yields can be considered as modest compared to that of *LLN* Coster-Kronig transitions. Broadening and shift of the observed *L* x rays originating from unresolved *N* satellite structures due to shakeoff processes may thus be disregarded.

A further examination of Table I shows that some of the transitions from highest occupied subshells have an unexpectedly large width which cannot be attributed to the effect of multiple vacancy states. Line shapes of the *L* transitions from the $5s_{1/2}$ and $5p_{3/2}$ orbitals are particularly influenced by this intriguing effect. As shown in Fig. 4, the $L_1$-$O_3$ transition is not only broadened but exhibits also a visible asymmetry on its low-energy flank. This asymmetry cannot be associated with *M* satellite components of the diagram line appearing just below since the latter is the $L_1$-$O_2$ transition. The same kind of deformation was observed for the $L_3$-$O_1$ line. In both cases, the complex profiles could be well fitted with two Voigtians separated by about 18 eV and labeled *I* and *II* in the tables. In a previous study concerning the *L* x-ray emission of uranium [11], very similar line shapes were obtained for these two transitions. The observed broadening and splitting of the transitions were interpreted as due to multiplet states formed by the exchange interaction between unpaired valence electrons and the core hole. More detailed information about this effect can be found in the paper by Hoszowska *et al.* [11].

The *L* x-ray energies of thorium determined in our work are listed in Table II. They are all based on the $K\alpha_1$ transition of gold measured in third order of reflection, i.e., at about the same Bragg angle as the transitions of interest. The energy ($68804.94 \pm 0.18$ eV) of this reference line was taken from Ref. [15]. In Table II the quoted uncertainties vary between 0.02 eV (1.2 ppm) for the strongest lines to about 1 eV (60 ppm) for the weakest ones. An additional relative uncertainty of about 3 ppm arising from the crystal lattice constant should be added to these numbers, whereas the errors inherent to the optical laser interferometer can be neglected. For comparison, in Table II we also report experimental values from Bearden [18] and Nordling and Hagström [32], as well as theoretical predictions from Larkins [33]. As Nordling and Hagström's data are based on x-ray photoemission spectroscopy (XPS) measurements, the transition energies were computed from the differences of the quoted binding energies. The same holds for the theoretical values from Larkins. In general we see from Table II that for the majority of the lines the three experimental values and the theoretical one are consistent within fluctuations of about $\pm 1$ eV. XPS results are, for most transitions, closer to ours than those from Bearden. It is also interesting to note that the calculated energies which reproduce quite well our results are, however, systematically higher by 1 eV or more for the $L_1$ transitions. This could be an indication that the binding energy of the $L_1$ level is overestimated by Larkins' calculations. This trend is not observed for the $L_2$ and $L_3$ transitions. Furthermore, we can see that our energy of the $L_1$-$O_2$ x-ray line is markedly smaller than the two other experimental values, the latter being both more or less consistent with the theoretical energy. Although no asymmetry such as the one observed in the $L_1$-$O_3$ and $L_3$-$O_1$ transitions could be detected in this line, we are inclined to explain the difference between our result and the three others by the exchange interaction effect mentioned above. The opposite is observed for the energy of the $L_1$-$P_{2,3}$ transition (Fig. 4), for which we have found a value higher by about 25 eV than the results of Bearden and Nordling and Hagström, but in satisfactory agreement with the theoretical prediction of Larkins. Using the binding energies quoted by Larkins for the $P_2$ (25 eV) and $P_3$ (17 eV) levels, energies of 20447 and 20455 eV are indeed obtained for the $L_1$-$P_2$ and $L_1$-$P_3$ transitions, values which are consistent with the result of 20450.4 eV found in the present work for the unresolved $L_1$-$P_{2,3}$ lines. For the $P_{2,3}$ doublet Nordling and Hagström gave a binding energy of 44 eV which is not confirmed by another more recent XPS measurement [34], from which values of 24.5 and 16.6 eV fully consistent with Larkins' predictions were obtained for the binding energies of the $P_2$ and $P_3$ levels. We are thus inclined to believe that the results of Bearden and Nordling and Hagström concerning the energy of the $L_1$-$P_{2,3}$ transition are erroneous.

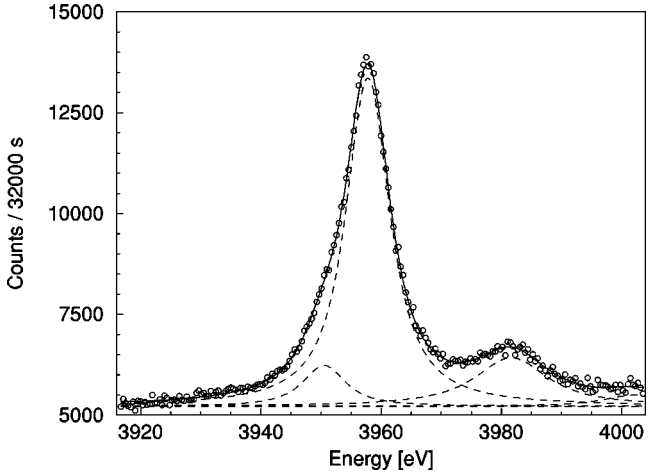


FIG. 5. The $M_3$-$O_{4,5}$ transitions of thorium at 3951 and 3958 eV, respectively, with the accompanying $N$ satellite structure.

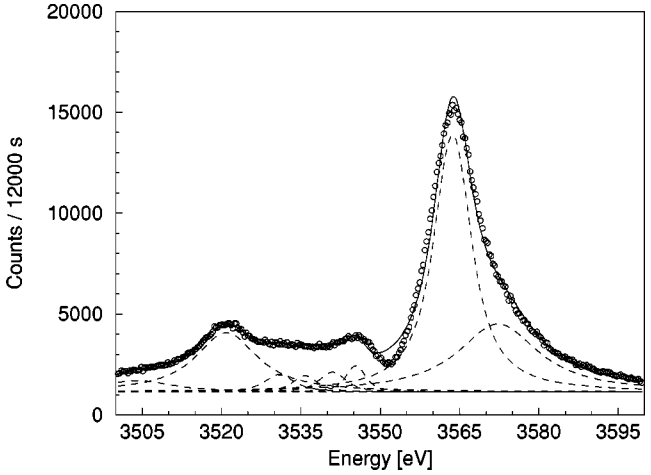


FIG. 7. The $M_3$-$N_{4,5}$ transitions of uranium at 3521 and 3564 eV, respectively, with the $M_3$-$N_5$ $N$ satellite structure at 3572 eV. One can see the influence of the $M_5$ absorption edge at 3553 eV. The broad structure between the $M_3$-$N_4$ line and the absorption edge corresponds to several overlapping transitions (see the text).

### B. *M* x-ray lines of thorium and uranium

One of the aims of the present project was the determination of the natural widths of the $L_1$ to $N_5$ atomic levels. However, to attain this objective the $L$ x-ray transition widths solely do not suffice. Additional information concerning the widths of the $M$ and $N$ levels is needed. The alternative would be to know the widths of several $M$ x-ray transitions from the $N$ shell. As existing experimental information concerning $M$ and $N$ level widths or $M$ x-ray linewidths is very scarce, our investigations were extended to the high-resolution observation of the $M$ x-ray emission spectra of thorium and uranium. Due to the poor intensity characterizing $M$ x rays, we have restricted our measurements to the strongest transitions. $M$ x-ray lines to the $M_1$ level which are extremely weak (for instance for thorium, the fluorescence yield $\omega_{M_1}$ is only $4.5\times10^{-3}$ [22]) could unfortunately not be observed for thorium nor for uranium.

For illustration the $M_3$-$O_{4,5}$ lines of thorium and the $M_5$-$N_{6,7}$ lines of uranium are depicted in Figs. 5 and 6, respectively. It is interesting to note that the $M_3$-$O_4$ and $M_5$-$N_6$ lines which correspond both to allowed $\Delta j=0$ $E1$ transitions are much weaker than the parent $\Delta j=1$ $M_3$-$O_5$ and $M_5$-$N_7$ transitions. A similar intensity attenuation for $\Delta j=0$ transitions is observed in $L$ x-ray spectra, as shown, for instance, in Fig. 2 for the $L_3$-$N_{4,5}$ transitions, but not in $K$ x-ray spectra where $\Delta j=0$ and 1 transitions have approximately the same transition probabilities. The more or less resolved structures observed on the high-energy side of the $M_3$-$O_5$ (Fig. 5) and $M_5$-$N_7$ (Fig. 6) diagram lines are due to $N$ satellites produced by $MMN$ Coster-Kronig transitions and to a smaller extent by shakeoff processes. It was mentioned in Sec. IV A that the energy shifts of the satellites associated with a given diagram line decrease with the principal quantum number of the spectator vacancies. It can also be shown that the satellite energy shifts increase with the principal quantum number of the transition electrons. This explains why the $N$ satellite structure is better separated from the parent diagram line for the $\Delta n=2$ $M_3$-$O_5$ transition than for the $\Delta n=1$ $M_5$-$N_7$ transition.

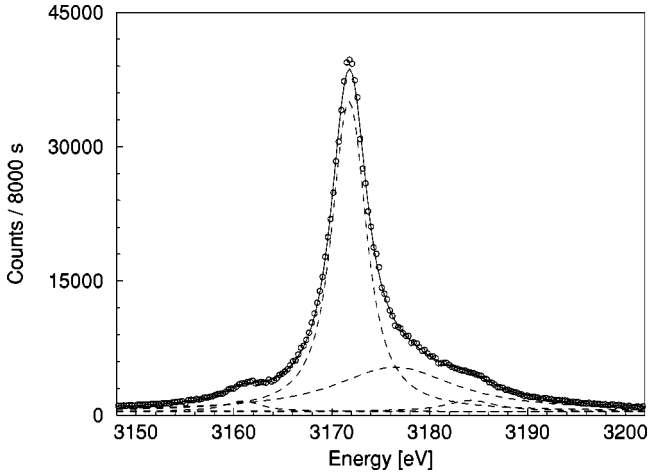


FIG. 6. The $M_5$-$N_{6,7}$ transitions of uranium at 3161 and 3172 eV, respectively, with the accompanying $N$ satellite structure components shifted by 5 and 13 eV with respect to the $M_5$-$N_7$ line.

The complexity of $M$ x-ray spectra and the difficulties encountered in their analysis are well illustrated by Fig. 7, which within a relatively narrow energy domain presents many $M$ x-ray lines of uranium. First one can see, at 3521 and 3563 eV, the $M_3$-$N_4$ and $M_3$-$N_5$ transitions, respectively. The asymmetry appearing on the high-energy flank of the $M_3$-$N_5$ line is due to the $N$ satellite of the latter transition. The small excess of intensity observed on the low-energy side of the $M_3$-$N_4$ line was attributed to the $M_5$-$P_1$ quadrupole transition, while the flat region between the $M_3$-$N_4$ and $M_3$-$N_5$ transitions consists of several unresolved lines that were tentatively assigned to the $M_3$-$N_4$ $N$ satellite and to the $M_4$-$O_3$ and $M_5$-$P_3$ transitions. The multiplet splitting found for the $L_1$-$O_3$ transition (see Sec. IV A) probably also affects the $M_4$-$O_3$ line, and thus contributes to the smearing of the spectral lines pertaining to this energy region. Furthermore,

TABLE III. Natural linewidths in (eV) of photoinduced $M$ x-ray emission lines of thorium. Our experimental results are compared to theoretical predictions from McGuire.

| Line | This experiment | Ref. [22,23] Calc. |
|---|---|---|
| $M_2$-$N_4$ | 17.7±0.2 | 20.8 |
| $M_3$-$N_5$ | 12.1±0.6 | 18.2 |
| $M_3$-$O_1$ | 40.0±2.1 | |
| $M_3$-$O_4$ | 7.5±0.8 | |
| $M_3$-$O_5$ | 7.7±0.1 | |
| $M_4$-$N_2$ | 16.5±1.4 | 11.5 |
| $M_4$-$N_6$ | 3.5±0.1 | 3.4 |
| $M_5$-$N_3$ | 14.3±0.7 | 10.4 |
| $M_5$-$N_6$ | 3.4±0.2 | 3.1 |
| $M_5$-$N_7$ | 3.5±0.1 | 3.1 |

the effect of the $M_5$ edge which results in an enhanced self-absorption of the x rays in the target is clearly visible around 3553 eV, where the experimental data are indeed poorly reproduced by the fit. The line shape of the $M_3$-$N_5$ transition is certainly affected by the close-lying $M_5$ edge. The linewidth obtained from the data analysis for this transition is indeed only 7.5±0.1 eV. This result, which is not consistent with the widths of the levels $M_3$ and $N_5$ extracted from the other $L$ and $M$ transitions is, in our opinion, not reliable, and was therefore not considered in the calculation of the $L_1$ to $N_5$ level widths (see Sec. IV C). It can be mentioned that we have not tried to correct the line shape of the $M_3$-$N_5$ transition to account for the increased self-absorption because, as observed in Ref. [35], the $M_5$ edge of U presents a complicated structure due to the resonant excitation of $3d$ electrons into the unfilled $5f$ subshell.

The linewidths and energies of the observed transitions are presented in Tables III and IV for thorium, and in Tables V and VI for uranium. The instrumental broadening of the von Hamos spectrometer was determined from measurements of several $K\alpha_1$ transitions whose linewidths were taken from Ref. [26]. As this instrumental broadening was small (about 1 eV) as compared to the linewidths of the $M$ x rays of interest, the errors (5–10 %) on the widths of the reference $K\alpha_1$ lines were neglected, and are thus not included in Tables III and V. No information concerning the energy shifts of $M$ x-ray lines with one spectator vacancy in the $O$ and $P$ shells could be found in the literature, except for the $M_4$-$N_6$ and $M_5$-$N_7$ transitions of uranium for which the theoretical energy shifts due to one spectator vacancy in the $O_1$ and $P_1$ subshells are reported in Ref. [36]. Values of 0.9 and 0.0 eV and 0.9 and 0.1 eV, respectively, are quoted for the two transitions. As these shifts are small as compared to the natural linewidths of the observed $M$ transitions, we have assumed that $O$ and $P$ satellites do not significantly influence the widths and energies of $M$ x rays. The theoretical linewidths were again obtained from the sum of the widths of the two levels involved in the transition. $M$ and $N$ levels widths were taken from McGuire's predictions (thorium $M$ levels

TABLE V. Natural linewidths in (eV) of photoinduced $M$ x-ray emission lines of uranium. Our experimental results are compared to existing experimental data (Expt.) and theoretical predictions (Calc.).

| Line | This experiment | Ref. [36] Expt. | Refs. [23,37] Calc. |
|---|---|---|---|
| $M_2$-$N_4$ | 18.1±0.2 | | 24.4 |
| $M_2$-$O_4$ | 18.7±0.3 | | 21.2 |
| $M_3$-$N_1$ | 20.2±0.8 | | 24.4 |
| $M_3$-$N_4$ | 13.4±0.3 | | 16.8 |
| $M_3$-$O_1$ | 38.4±3.2 | | |
| $M_3$-$O_4$ | 8.1±1.0 | | |
| $M_3$-$O_5$ | 8.2±0.1 | | |
| $M_4$-$N_2$ | 15.3±1.0 | 13±2 | 11.9 |
| $M_4$-$N_6$ | 3.6±0.1 | 4.3±0.3 | 4.7 |
| $M_5$-$N_3$ | 12.8±0.3 | 15±2 | 10.8 |
| $M_5$-$N_6$ | 3.6±0.1 | 4.1±0.6 | 4.5 |
| $M_5$-$N_7$ | 3.5±0.1 | 4.1±0.3 | 4.5 |

TABLE IV. Energies in (eV) of photoinduced $M$ x-ray emission lines of thorium. Our experimental results are compared to the data from two experiments (Expt.) and one theory (Calc.).

| Line | This experiment | Ref. [18] Expt. | Ref. [32] Expt. | Ref. [33] Calc. |
|---|---|---|---|---|
| $M_2$-$N_4$ | 4116.0±0.1 [a] | 4117.0 | 4116.2 | 4117.0 |
| $M_3$-$N_5$ | 3370.3±0.1 [b] | 3370.0 | 3369.7 | 3369.0 |
| $M_3$-$O_1$ | 3751.9±0.5 [c] | 3780.0 | 3756.0 | 3756.0 |
| $M_3$-$O_4$ | 3950.5±0.3 [c] | | 3951.6 | 3951.0 |
| $M_3$-$O_5$ | 3957.8±0.1 [c] | | 3957.9 | 3959.0 |
| $M_4$-$N_2$ | 2323.1±0.3 [b] | 2322.0 | 2322.4 | 2323.0 |
| $M_4$-$N_6$ | 3147.0±0.1 [b] | 3145.8 | 3146.6 | 3147.0 |
| $M_5$-$N_3$ | 2365.2±0.3 [b] | 2364.0 | 2364.5 | 2364.0 |
| $M_5$-$N_6$ | 2988.0±0.1 [b] | 2987.0 | 2987.9 | 2988.0 |
| $M_5$-$N_7$ | 2997.0±0.1 [b] | 2996.1 | 2997.1 | 2997.0 |

[a]Reference energy 4090.6 eV (Sc $K\alpha_1$).
[b]Reference energy 2957.70 eV (Ar $K\alpha_1$).
[c]Reference energy 3691.68 eV (Ca $K\alpha_1$).

TABLE VI. Energies in (eV) of photoinduced $M$ x-ray emission lines of uranium. Our results are compared to the data from three experiments (Expt.) and one theory (Calc.).

| Line | This experiment | Ref. [18] Expt. | Ref. [36] Expt. | Ref. [38] Expt. | Ref. [33] Calc. |
|---|---|---|---|---|---|
| $M_2$-$N_4$ | 4400.8±0.1 [a] | 4401.0 | | 4401.0 | 4401.0 |
| $M_2$-$O_4$ | 5075.9±0.1 [b] | 5075.0 | | | 5078.0 |
| $M_3$-$N_1$ | 2863.0±0.1 [c] | 2863.0 | | 2862.2 | 2862.0 |
| $M_3$-$N_4$ | 3521.0±0.1 [d] | 3521.0 | | 3523.7 | 3524.0 |
| $M_3$-$O_1$ | 3979.9±0.3 [e] | 3980.0 | | | 3980.0 |
| $M_3$-$O_4$ | 4195.8±0.4 [e] | | | | 4201.0 |
| $M_3$-$O_5$ | 4204.2±0.1 [e] | | | | 4208.0 |
| $M_4$-$N_2$ | 2455.6±0.2 [c] | 2454.8 | 2455.7 | 2455.4 | 2455.0 |
| $M_4$-$N_6$ | 3336.7±0.1 [c] | 3336.7 | 3336.7 | | 3336.0 |
| $M_5$-$N_3$ | 2507.0±0.1 [c] | 2507.0 | 2506.8 | 2506.6 | 2507.0 |
| $M_5$-$N_6$ | 3160.9±0.1 [c] | 3159.5 | 3160.0 | | 3160.0 |
| $M_5$-$N_7$ | 3171.8±0.1 [c] | 3170.8 | 3171.4 | | 3172.0 |

[a]Reference energy 4510.84 eV (Ti $K\alpha_1$).
[b]Reference energy 4952.20 eV (V $K\alpha_1$).
[c]Reference energy 2957.70 eV (Ar $K\alpha_1$).
[d]Reference energy 3691.68 eV (Ca $K\alpha_1$).
[e]Reference energy 4090.6 keV (Sc $K\alpha_1$).

[22], uranium $M$ levels [37], and thorium and uranium $N$ levels [23]). To our knowledge experimental information concerning $M$ x-ray linewidths does not exist for thorium, whereas for uranium some data were found for the $M_4$ and $M_5$ transitions [36]. Regarding the energies, experimental results are available for both thorium and uranium but not for all transitions. As for the $L$ x rays, the theoretical energies of the $M$ x-ray lines were computed from the binding energies quoted by Larkins [33].

A comparison of the linewidths obtained in our experiment with McGuire's predictions shows that the theoretical values systematically overestimate the widths of the transitions to the $M_2$ and $M_3$ levels. This observation may indicate that McGuire's probabilities for $M_2M_4X$ and $M_3M_5X$ Coster-Kronig transitions which are the predominant processes in the decay of $M_2$ and $M_3$ vacancies are too large. Thus it seems that the rates of the $N_2N_4X$ and $N_3N_5X$ Coster-Kronig transitions which govern the $N_2$ and $N_3$ vacancy lifetimes are underestimated by the calculations of McGuire. This statement is based on the fact that McGuire's predictions for the $M_4$-$N_2$ and $M_5$-$N_3$ transitions are smaller by 3–5 eV than our experimental values, whereas his predictions for the $M_4$-$N_6$, $M_5$-$N_6$, and $M_5$-$N_7$ transitions are in satisfactory agreement with our results. Concerning the experimental linewidths given by Keski-Rahkonen and Krause [36] for two $M_4$ and three $M_5$ x-ray lines of uranium, one can see from Table V that relative differences up to 15% are found, but the quoted values are almost consistent with ours within the given experimental uncertainties.

The energies found in the present work for the $M$ x-ray lines of thorium and uranium are based on the energies of different $K\alpha_1$ transitions from several light elements (see Tables IV and VI for details). The errors on the energies taken as references are typically of the order of 10 ppm, but they are not included in the uncertainties quoted in Tables IV and VI. Except for the $M_3$-$O_1$ transition, our results are remarkably well reproduced by Larkins calculations [33] in the case of thorium. For uranium, the energies of the $M_2$-$O_4$, $M_3$-$O_4$, and $M_3$-$O_5$ transitions are overestimated by the theory by 2–5 eV, indicating that the $O_4$ and $O_5$ binding energies of Larkins are probably too large. Energies of other transitions, however, are in good agreement with our results. Extending the comparison to other existing experimental data, we see that in general the agreement is excellent for uranium with one exception concerning the energy of the $M_3$-$N_4$ transition quoted by Nordling and Hagström [38]. In the case of thorium, an overall agreement is also found especially with the results given by Nordling and Hagström, but two strong discrepancies are found for the energies quoted by Bearden for the $M_3$-$O_1$ and $M_3$-$O_4$ lines. The latter are probably wrong since our energies are almost consistent with the XPS results from Refs. [32] and [34] and with the theoretical values of Larkins.

### C. Level widths of subshells $L_1$ to $N_5$

The natural width of an x-ray line represents the sum of the widths of the two atomic levels participating in the transition. As a consequence one can build from the linewidths of the measured $L$ and $M$ x-ray lines a set of $n$ simultaneous equations with $m$ level widths as unknowns. If $n>m$, as in our case, the set of equations can be solved by means of a least-squares method. However, because most transitions from the outer $O$ and $P$ shells are influenced by nonlifetime broadening effects, only those transitions that involve the $L_1$ to $N_7$ subshells should enter the set of equations.

The widths of the $N_6$ and $N_7$ levels are expected to be nearly equal [39] and small (about 0.3 eV for uranium according to Ref. [36]). Thus, they cannot be extracted in a reliable way from $M$-$N_{6,7}$ and $L$-$N_{6,7}$ x-ray lines whose line-

TABLE VII. Atomic level widths in (eV) of subshells $L_1$ to $N_5$ of thorium. Our experimental results are compared with theoretical predictions from McGuire [21–23], and Chen *et al.* [41,42], semiempirical data from Krause and Oliver [26], and fitted data from Campbell and Papp [39].

| Subshell | This work | Refs. [21–23] | Refs. [41,42] | Ref. [26] | Ref. [39] |
|---|---|---|---|---|---|
| $L_1$ | 14.3±0.2 | 20.4 | 15.8 | 13.7 | 14.7 |
| $L_2$ | 8.5±0.1 | 11.3 | 7.7 | 8.2 | 8.0 |
| $L_3$ | 8.4±0.1 | 7.0 | 7.7 | 7.1 | 7.5 |
| $M_1$ | 14.6±0.2 | 22.7 | 19.3 | | 18.4 |
| $M_2$ | 13.2±0.2 | 15.5 | 14.5 | | 14.3 |
| $M_3$ | 7.9±0.2 | 12.9 | 10.1 | | 7.7 |
| $M_4$ | 3.3±0.1 | 3.2 | | | 3.3 |
| $M_5$ | 3.4±0.1 | 2.9 | | | 3.2 |
| $N_1$ | 10.9±0.1 | 11.2 | | | 11.1 |
| $N_2$ | 9.0±0.2 | 8.3 | | | 8.9 |
| $N_3$ | 8.4±0.2 | 7.5 | | | 7.5 |
| $N_4$ | 4.5±0.1 | 5.3 | | | 4.1 |
| $N_5$ | 4.1±0.1 | 5.3 | | | 4.1 |

widths are 10–30 times larger. For this reason the $N_{6,7}$ level widths of thorium and uranium were fixed at 0.15 and 0.29 eV, respectively, in the least-squares method. These values were taken from McGuire [23]. They were preferred to the XPS widths from Fuggle and Alvarado [40] because the latter, which are about 0.4 eV larger, are most likely affected by exchange splitting. Furthermore, as noticed by Campbell and Papp [39], calculations based on the single-particle model (SPM) as those of McGuire reproduce well the experimental $N_7$ level widths in the region $70 \leqslant Z \leqslant 83$. Such SPM predictions should thus also be valid for $Z > 83$.

For uranium we have used the $L$ x-ray linewidths reported by Hoszowska *et al.* [11], except for the $L_3$-$M_4$, $L_3$-$M_5$, and $L_3$-$N_5$ transitions, whose widths were taken from the experimental data of Amorim *et al.* [25]. Amorim *et al.*'s results are indeed closer to the least-squares-fit to existing experimental data of Campbell and Papp [39] than those of Hoszowska *et al.* for these specific transitions.

If one restricts the least-squares method to the transitions involving the $L_1$ to $N_7$ levels, the $M_3$ subshell width enters the set of equations only via the $L_1$-$M_3$ and $M_3$-$N_5$ transitions. In the first transition, however, the linewidth is due mainly to the broad $L_1$ level, and the corresponding equation is thus not very sensitive to the $M_3$ level width. Regarding the second transition, the experimental uncertainty on the linewidth (0.6 eV) is relatively large so that the influence of this line on the $M_3$ level width determined by the weighted least-squares fit is also only moderate. For these reasons we have added in the sets of equations corresponding to thorium and uranium the $M_3$-$O_5$ transitions, taking for the $O_5$ level width the XPS values ($0.6 \pm 0.2$ eV for thorium and $1.1 \pm 0.3$ eV for uranium) reported by Fuggle and Alvarado [40]. In this respect, it can be mentioned further that, in contrast to $O_{1-3}$ subshells, the $O_5$ level seems to be not affected by exchange splitting or solid state effects since no broadening nor asymmetry was observed in any of the $L$ or $M$ x-ray transitions from the $O_5$ level.

From the $L$ and $M$ x-ray linewidths determined in the present work and the ones discussed above, two sets of 29 equations for thorium and 30 for uranium were obtained with 13 unknowns corresponding to the widths of the levels $L_1$ to $N_5$. The sets of simultaneous linear equations were solved by minimizing the sums of the weighted squares of deviations. Weighting factors inversely proportional to the experimental errors and not to the squares of the latter were employed in order to give more consideration in the fit to the influence of weaker transitions. The so-obtained level widths are presented for thorium and uranium in Tables VII and VIII, respectively, where they are compared to results based on least-squares fits to existing experimental data from Campbell and Papp [39] and to theoretical predictions from McGuire [21–23,37] and Chen *et al.* [41–43]. The semiempirical values reported by Krause and Oliver [26] for the subshells $L_1$ to $L_3$ are included in the tables.

In the careful and extensive compilation of existing experimental level widths reported by Campbell and Papp [39], most results are presented graphically and errors concerning their fits to available experimental data are in most cases not mentioned. However, if we assume an average relative uncertainty of about 5% for their results, one can see from Tables VII and VIII that our level widths are consistent with those of Campbell and Papp for all thorium and uranium subshells, except for the $L_3$ and $M_1$ subshells. Actually, the $L_3$ level width determined in our work seems to be too large by about 0.5–1.0 eV. This could indicate that the nonlifetime broadening induced by the unresolved $N$ satellites originating from $L_jL_3N$ Coster-Kronig transitions is not as unimportant as anticipated. The larger discrepancy observed for the $M_1$ level width is more difficult to understand. The values deduced from our experiment are indeed 3.8 eV for thorium and 3.0 eV for uranium, smaller than the fitted values from Campbell and Papp. One could argue that the discrepancy is due to the least-squares method itself, because in the latter the determination of the $M_1$ level width is only anchored to

TABLE VIII. Atomic level widths in (eV) of subshells $L_1$ to $N_5$ of uranium. Our experimental results are compared with theoretical predictions from McGuire [21–23,37] and Chen *et al.* [41–43], semiempirical data from Krause and Oliver [26], and fitted data from Campbell and Papp [39].

| Subshell | This work | Refs. [23,37] | Refs. [41–43] | Ref. [26] | Ref. [39] |
|---|---|---|---|---|---|
| $L_1$ | 16.0±0.2 | 19.3 | 16.5 | 14.0 | 15.5 |
| $L_2$ | 10.0±0.1 | 10.9 | 8.6 | 9.3 | 9.3 |
| $L_3$ | 8.4±0.2 | 7.3 | 8.2 | 7.4 | 7.9 |
| $M_1$ | 15.5±0.2 | 23.0 | 19.5 | | 18.5 |
| $M_2$ | 14.1±0.2 | 20.2 | 14.7 | | 15.0 |
| $M_3$ | 7.9±0.2 | 12.6 | 10.4 | | 7.5 |
| $M_4$ | 3.2±0.1 | 4.5 | 3.7 | | 3.5 |
| $M_5$ | 3.3±0.1 | 4.2 | 3.6 | | 3.5 |
| $N_1$ | 12.6±0.2 | 11.8 | | | 11.5 |
| $N_2$ | 9.7±0.2 | 7.5 | | | 9.5 |
| $N_3$ | 8.7±0.2 | 6.6 | | | 8.1 |
| $N_4$ | 4.7±0.1 | 4.2 | | | 4.2 |
| $N_5$ | 4.2±0.6 | 4.2 | | | 4.2 |

the $L_3$-$M_1$ and $L_2$-$M_1$ transitions. This argument looks reasonable but, in our opinion, it does not completely clarify the question. The widths of the $L_3$-$M_1$ and $L_2$-$M_1$ transitions in thorium computed from the level widths quoted by Campbell and Papp are 25.9 and 26.4 eV, respectively, i.e., 2.3 and 3.3 eV larger than the values obtained in our study. This is intriguing because, on the one hand, the differences are more than tens times larger than the experimental errors and on the other hand because it is difficult to find plausible reasons explaining why observed spectral lines would be too narrow. A too large value of the instrumental broadening indeed cannot account for the observed differences, because in that energy region the instrumental width is only 3.5 eV. Furthermore, if the $M_1$ widths are kept fixed in the least-squares method at the values quoted by Campbell and Papp, the widths given by the fit for the other levels are in poorer agreement than in the case where the $M_1$ widths are used as free parameters. For all these reasons we are not convinced that the $M_1$ level widths of thorium and uranium obtained from our experiment are really too small.

The relative uncertainties estimated by Krause and Oliver [26] for their semiempirical level widths are 20%, 10%, and 8%, respectively, for the $L_1$, $L_2$, and $L_3$ subshells. Comparing their values with our results, we observe again a good agreement for the $L_1$ and $L_2$ levels, whereas our $L_3$ level widths of thorium and uranium exceed Krause-Oliver data by 15% and 12%, respectively. Values from Campbell and Papp for the $L_3$ subshell are also larger than those of Krause and Oliver, but they agree within the quoted uncertainty of 8%.

Larger discrepancies are observed when comparing our results to McGuire's predictions for the $L$ [21,37], $M$ [22,37], and $N$ [23] level widths. Except for three levels of thorium ($L_3$, $M_4$, and $M_5$) and one of uranium ($L_3$), the predictions overestimate our results and those of Campbell and Papp for the $L_1$ to $M_5$ levels. The deviations are the largest for the $L_1$ and $M_1$ subshells, where they reach about 40%, indicating, as already mentioned in Sec. IV A, that McGuire's $LLX$ and $MMX$ Coster-Kronig yields are significantly overestimated. For the $N_1$ to $N_5$ levels, one observes an opposite trend of the theory which underestimates the experimental widths.

Relativistic independent particle calculations concerning atomic level widths were also performed by Chen and Crasemann. For thorium, results are only available for the $L_1$ to $M_3$ core levels [41,42]. For uranium predictions exist for the $L_1$ to $M_5$ subshells [41–43]. In Ref. [42] Chen *et al.* mentioned that their calculations overestimate the $M_{2,3}$ and $M_1$ Coster-Kronig rates in heavy atoms by $\sim$10–15 % and $\sim$30–50 %, respectively. This statement is confirmed by our results which show in addition that the overestimation is larger for the $M_3$ level than for the $M_2$ one. In general, however, the results of Chen *et al.* are noticeably closer to the experimental values than those of McGuire.

Finally, in Table IX, the $N_4$ and $N_5$ level widths of thorium and uranium extracted from our measurements are compared to calculations performed by Ohno and Wendin [44] within the frame of a nonrelativistic many-body theory. The predictions were computed from two different approaches. In the so-called A1 approximation, a frozen-core potential and frozen Auger energy were used, while in the A2 approximation a frozen-core potential but relaxed and

TABLE IX. $N_4$ and $N_5$ level widths in (eV). Our experimental results are compared with theoretical predictions of Ohno and Wendin [44]. The A1 approximation uses the frozen-core potential and frozen Auger energy, and the A2 approximation uses the frozen-core potential and relaxed and relativistic Auger energies.

| | Thorium | | | Uranium | | |
|---|---|---|---|---|---|---|
| | | Theory | | | Theory | |
| Level | Present | A1 | A2 | Present | A1 | A2 |
| $N_4$ | 4.54±0.13 | 4.63 | 3.49 | 4.70±0.11 | 4.69 | 3.61 |
| $N_5$ | 4.06±0.13 | 4.63 | 3.90 | 4.15±0.61 | 4.69 | 3.73 |

relativistic Auger energy were employed. From the comparison one sees that for both thorium and uranium our $N_4$ level widths are better reproduced by the A1 approximation, whereas for the $N_5$ subshell our experimental results are between the predictions corresponding to the two approximations. Ohno-Wendin calculations based on the same many-body model also exist for the $N_1$, $N_2$, and $N_3$ level widths. However, in the high-$Z$ region, results are only available for mercury. These results were compared with XPS data from Svensson *et al.* [45]. A quite satisfactory agreement was found.

## ACKNOWLEDGMENT

This work was partly supported by the Swiss National Science Foundation.

[1] M. Budnar and A. Mühleisen, Nucl. Instrum. Methods Phys. Res. B **75**, 81 (1993).
[2] J. A. Maxwell, W. J. Teesdale, and J. L. Campbell, Nucl. Instrum. Methods Phys. Res. B **43**, 218 (1989).
[3] J. L. Campbell, Nucl. Instrum. Methods Phys. Res. B **49**, 115 (1990).
[4] T. Åberg, in *Atomic Inner-Shell Processes*, edited by B. Crasemann (Academic Press, New York, 1975), p. 353.
[5] Ch. Herren and J.-Cl. Dousse, Phys. Rev. A **53**, 717 (1996).
[6] A. Mühleisen, M. Budnar, and J.-Cl. Dousse, Phys. Rev. A **54**, 3852 (1996).
[7] Ch. Herren and J.-Cl. Dousse, Phys. Rev. A **56**, 2750 (1997).
[8] A. Mühleisen, M. Budnar, J.-Cl. Dousse, J. Hoszowska, and Z. G. Zhao, X-Ray Spectrom. **27**, 337 (1998).
[9] J.-Cl. Dousse and J. Hoszowska, Phys. Rev. A **56**, 4517 (1997).
[10] T. Papp, J. L. Campbell, J. A. Maxwell, J.-X. Wang, and W. J. Teesdale, Phys. Rev. A **45**, 1711 (1992).
[11] J. Hoszowska, J.-Cl. Dousse, and Ch. Rhême, Phys. Rev. A **50**, 123 (1994).
[12] B. Galley and J.-Cl. Dousse, Phys. Rev. A **50**, 3058 (1994).
[13] W. Beer, P. F. A. Goudsmit, and L. Knecht, Nucl. Instrum. Methods Phys. Res. A **219**, 322 (1984).
[14] W. Schwitz, Nucl. Instrum. Methods **154**, 95 (1978).
[15] E. G. Kessler, Jr., R. D. Deslattes, D. Girard, W. Schwitz, L. Jacobs, and O. Renner, Phys. Rev. A **26**, 2696 (1982).
[16] J. Hoszowska, J.-Cl. Dousse, J. Kern, and Ch. Rhême, Nucl. Instrum. Methods Phys. Res. A **376**, 129 (1996).
[17] S. I. Salem and P. L. Lee, At. Data Nucl. Data Tables **18**, 233 (1976).
[18] J. A. Bearden, Rev. Mod. Phys. **39**, 78 (1967).
[19] F. James and M. Roos, Comput. Phys. Commun. **10**, 343 (1975).
[20] W. Uchai, C. W. Nestor, Jr., S. Raman, and C. R. Vane, At. Data Nucl. Data Tables **34**, 201 (1986).
[21] E. J. McGuire, Phys. Rev. A **3**, 587 (1971).
[22] E. J. McGuire, Phys. Rev. A **5**, 1043 (1972).
[23] E. J. McGuire, Phys. Rev. A **9**, 1840 (1974).
[24] J. Merill and J. W. M. DuMond, Ann. Phys. (N.Y.) **14**, 166 (1961).
[25] P. Amorim, L. Salgueiro, F. Parente, and J. G. Ferreira, J. Phys. B **21**, 3851 (1988).
[26] M. O. Krause and J. H. Oliver, J. Phys. Chem. Ref. Data **8**, 328 (1979).
[27] F. Parente, M. H. Chen, B. Crasemann, and H. Mark, At. Data Nucl. Data Tables **26**, 383 (1981).
[28] M. H. Chen, B. Crasemann, and H. Mark, At. Data Nucl. Data Tables **24**, 13 (1979).
[29] F. Parente, M. L. Carvalho, and L. Salgueiro, J. Phys. B **16**, 4305 (1983).
[30] T. Åberg, Phys. Rev. A **156**, 35 (1967).
[31] T. A. Carlson and C. W. Nestor, Jr., Phys. Rev. A **8**, 2887 (1973).
[32] C. Nordling and S. Hagström, Z. Phys. **178**, 418 (1964).
[33] F. P. Larkins, At. Data Nucl. Data Tables **20**, 319 (1977).
[34] J. C. Fuggle and N. Mårtensson, J. Electron Spectrosc. Relat. Phenom. **21**, 275 (1980).
[35] C. Bonnelle and G. Lachère, J. Phys. (Paris) **35**, 295 (1974).
[36] O. Keski-Rahkonen and M. O. Krause, Phys. Rev. A **15**, 959 (1977).
[37] E. J. McGuire, in *Proceedings of the International Conference on Inner Shell Ionization Phenomena and Future Applications, Atlanta, Georgia, 1972*, edited by R. W. Flink, S. T. Manson, J. M. Palms, and P. V. Rao (Natl. Tech. Information Service, U.S. Dept. of Commerce, Springfield, VA, 1973), p. 662.
[38] C. Nordling and S. Hagström, Ark. Fys. **15**, 431 (1959).
[39] J. L. Campbell and T. Papp, X-Ray Spectrom. **24**, 307 (1995).
[40] J. C. Fuggle and S. F. Alvarado, Phys. Rev. A **22**, 1615 (1980).
[41] M. H. Chen, B. Crasemann, and H. Mark, Phys. Rev. A **24**, 177 (1981).
[42] M. H. Chen, B. Crasemann, and H. Mark, Phys. Rev. A **27**, 2989 (1983).
[43] M. H. Chen, B. Crasemann, and H. Mark, Phys. Rev. A **21**, 449 (1980).
[44] M. Ohno and G. Wendin, Phys. Rev. A **31**, 2318 (1985).
[45] S. Svensson, N. Mårtensson, E. Basilier, P. Å. Malmquist, U. Gelius, and K. Siegbahn, J. Electron Spectrosc. Relat. Phenom. **9**, 51 (1976).